Inorganic Chemistry

ARTICLE

pubs.acs.org/IC

Interplay among Aromaticity, Magnetism, and Nonlinear Optical Response in All-Metal Aromatic Systems

Satadal Paul and Anirban Misra*

Department of Chemistry, University of North Bengal, Darjeeling, PIN 734 013, West Bengal, India

Supporting Information

ABSTRACT: All-metal aromatic molecules are the latest inclusion in the family of aromatic systems. Two different classes of all-metal aromatic clusters are primarily identified: one is aromatic only in the low spin state, and the other shows aromaticity even in high-spin situations. This observation prompts us to investigate the effect of spin multiplicity on aromaticity, taking Al_4^{2-}, $Te_2As_2^{2-}$, and their copper complexes as reference systems. Among these clusters, it has been found that the molecules that are aromatic only in their singlet state manifest antiaromaticity in their triplet state. The aromaticity in the singlet state is characterized by the diatropic ring current circulated through the bonds, which are cleaved to generate excess spin density on the atoms in the antiaromatic triplet state. Hence, in such systems, an antagonistic relationship between aromaticity and high-spin situations emerges. On the other hand, in the case of triplet aromatic molecules, the magnetic orbitals and the orbitals maintaining aromaticity are different; hence, aromaticity is not depleted in the high-spin state. The nonlinear optical (NLO) behavior of the same set of clusters in different spin states has also been addressed. We correlate the second hyperpolarizability and spin density in order to judge the effect of spin multiplicity on third-order NLO response. This correlation reveals a high degree of NLO behavior in systems with excess spin density. The variance of aromaticity and NLO response with spin multiplicity is found to stem from a single aspect, the energy gap between the highest occupied molecular orbital (HOMO) and the lowest unoccupied molecular orbital (LUMO), and eventually the interplay among aromaticity, magnetism, and NLO response in such materials is established. Hence, the HOMO−LUMO energy gap becomes the cornerstone for tuning the interplay. This correlation among the said properties is not system-specific and thus can be envisaged even beyond the periphery of all-metal aromatic clusters. Such interplay is of crucial importance in tailoring novel paradigm of multifunctional materials.

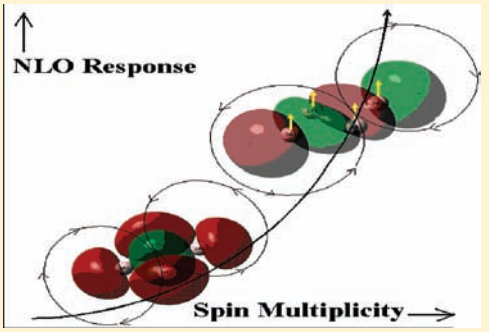

INTRODUCTION

The isolation and characterization of MAl_4^{2-} (M = Na, K, Cu) by Li et al. is a breakthrough in the concept of aromatic compounds.[1a] This series of bimetallic clusters is found to have square-planar Al_4^{2-}, which has been confirmed to have aromaticity through photoelectron spectroscopic investigation and electronic structure analysis by ab initio calculations. This finding sparked interest among researchers to investigate the domain of all-metal aromatic systems (AMASs). There are numerous reports on aromaticity in all-metal clusters, whose stabilities are verified through experimental or theoretical studies.[1−13] These systems include XAl_3^- (X = Si, Ge, Sn, Pb),[2] M_4^{2-} (M = Ga, In, Tl, Sb, Bi),[3] T_5^{6-} (T = Ge, Sn, Pb),[4] M_4^{2+} (M = Se, Te),[5] M^{3-} (M = Al, Ga),[6] Al_6^{2-},[7] Hg_4,[5,8] M_5^- (M = Sb, Bi),[9] Au_5Zn^+,[10] Cu_3^{3+},[11] Cu_4^{2-},[12] $[Fe(X_5)]^+$ (X = Sb, Bi),[13] and so on. A detailed explanation of the stability and reactivity of a wide range of all-metal aromatic and antiaromatic systems has been given by Chattaraj and co-workers on the basis of density functional theory calculations.[14] Aromatic systems have a usual inclination to form coordination bonds with metals through their dispersed electron cloud. Mercero, Ugalde, and co-workers theoretically verified the possibility of such complexes with AMASs and demonstrated that the all-metal aromatic Al_4^{2-} deck can be used to sandwich transition-metal atoms.[15] Another possibility of such a complex is explored by sandwiching transition metals between aromatic As_4^{2-} decks.[16] These works, in fact, invoke the synthesis of novel all-metal metallocenes. Yang et al. further extended this idea of such sandwich complexes with main-group metals.[17]

The origin of aromaticity in such metal clusters can be explained through the Hückel $(4n + 2)$ π electron rule.[1−15] Other than this simple electron count rule, the aromatic character of these metal cluster ions has also been diagnosed through their response toward the magnetic field. The ability to sustain a diamagnetic ring current induced by a perpendicular magnetic field has been considered as the magnetic criterion of aromaticity.[18] Because "diatropicity" is synonymous with "aromaticity", relying on a similar argument, it has been suggested by many authors that "paratropicity" implies "antiaromaticity".[19] The diatropic (paratropic) ring current may be maintained by circulation of either π- or σ-bonded electrons, and the system is termed as π-aromatic (π-antiaromatic) or σ-aromatic

Received: August 15, 2010
Published: March 11, 2011

(σ-antiaromatic) accordingly. The AMASs exhibit somewhat different trends in their magnetic properties in comparison with organic aromatic and antiaromatic compounds.[20−22] The diamagnetic ring current is found to be produced in Al_4^{2-} by the magnetic-field-induced σ-electron circulation as well as the π-electron circulation, and this simultaneous σ and π aromaticity is termed multiple aromaticity.[1c,15] However, Fowler and co-workers argued for only σ aromaticity in Al_4^{2-} through ab initio analysis.[20] On the other hand, π-electron circulation may induce a paramagnetic ring current out of the plane, which makes all-metal clusters π-antiaromatic.[21,22] For example, in rectangular Al_4^{4-}, a paratropic ring current above the rectangular plane defines it as π-antiaromatic (as is also indicated by the presence of $4n$ electrons) and a concurrent diatropic ring current in the plane of the ring makes it σ-aromatic.[1c] $Li_3Al_4^-$ is also found to have a concurrent existence of σ aromaticity and π antiaromaticity, which is termed as conflicting aromaticity.[1c,23] The occurrence of such uncommon multiple and conflicting aromaticity in AMASs puts an impetus in investigating their magnetic criterion of aromaticity.

The nonlinear optical (NLO) properties of AMASs have also been a subject of current interest,[24−26] which has actually been triggered by the observation of exceptionally high NLO response for small clusters functionalized with various metals.[24a] Organic π-conjugated polymers show an increase in their second- and third-order NLO response, β and γ, with their conjugation length.[27] Again there are reports on an increase in the radicaloid character with an increase in the conjugation length of π-conjugated systems.[28] Thus, it can be intuited that NLO response will increase with an increase in the radicaloid character. Nakano et al. pointed out that NLO response is drastically affected by the spin multiplicity, particularly in singlet systems with intermediate diradical character.[29] Singlet compounds with intermediate diradical characters are found to exhibit larger second hyperpolarizability than their corresponding triplet counterparts.[29a] Also, in some other works, they observed NLO response to amplify monotonically with spin multiplicity.[29c] This observation is in agreement with the fact that systems with reduced energy gaps between the highest occupied molecular orbital (HOMO) and the lowest unoccupied molecular orbital (LUMO) have an increased NLO response.[30] In this context, it becomes significant to evoke the fact that the reduced HOMO−LUMO energy gap (ΔE_{HL}) is also the signature of antiaromaticity.[31] In contrast, aromaticity is found to be associated with large ΔE_{HL}. This relationship of aromaticity and antiaromaticity with ΔE_{HL} has been the subject of several studies.[32]

The parameter ΔE_{HL}, simultaneously affecting aromaticity, magnetism, and NLO response, thus bequeaths a hint of a strong connection among these properties in all-metal clusters. Such interplay among a miscellany of properties may provide an innovative route to the design of materials with multiple properties. The simultaneous existence of various functionalities in a single entity can play a pivotal role in meeting the needs of a fast growing technology for their potentiality to act as molecular switches with tunable properties. The bottleneck in the development of such multifunctional molecules is the lack of some common origin, wherefrom all of the properties may generate. For instance, NLO response is traditionally regarded within the framework of dielectrics subjected to intense electric fields and magnetism is a manifestation of interaction among spins, and that is why, rationale for linking NLO and magnetism in a single molecule is difficult to find.[33] However, from the above discussion, ΔE_{HL} appears to be connected with the discussed properties, and thus a link among them can be anticipated. In fact, the antiferromagnetic and ferromagnetic states exhibit different NLO effects, and this strongly hints about the connection between NLO response with the magnetic behavior of the molecule.[34] There are also reports of materials with combined properties such as conductivity and magnetism,[35] conductivity and NLO behavior,[36] or magnetism and NLO properties.[37]

The unique nature of aromaticity and the ability to produce a high value of NLO response in AMASs, as is apparent from the preceding discussion, catch our interest to correlate these two aspects therein. These properties are found to vary with the HOMO−LUMO energy gap, which is also a crucial parameter for controlling the spin multiplicity of any system. Hence, the variance in aromaticity and NLO response with spin multiplicity emerges as the primary focus of this work. Because spin multiplicity describes the magnetic nature of any system, this study eventually offers a description of the interplay among aromaticity, magnetism, and NLO response. Aromaticity of Al_4^{2-} in the singlet ground state is much cultivated. In contrast, $Te_2As_2^{2-}$, a part of the molecule $[K(18\text{-crown-}6)]_2[Te_2As_2]$, recently synthesized by Khanna and co-workers, is claimed to be the first aromatic as well as ferromagnetic compound.[38] This divergent aromaticity in the singlet ground state of Al_4^{2-} and the triplet ground state of $Te_2As_2^{2-}$ urges their selection as reference systems in this work. When complexed with alkali metals, Al_4^{2-} shows an exaltation in nonlinearity because of charge transfer from the alkali metals to the Al_4^{2-} ring.[24] There are many other instances where charge transfer induces a high degree of NLO response probably because of a large charge fluctuation.[39] Moreover; if transition metals are used for complexation, it provides an opportunity to investigate any change in the magnetic nature of the aromatic ring through interaction with unpaired electrons of the transition metals. Stabilization of such clusters by complexation with transition metals is already fortified theoretically.[40] All of these aspects prompt us also to extend this theoretical study with copper complexes of Al_4^{2-} and $Te_2As_2^{2-}$.

THEORETICAL DETAILS AND METHODOLOGY

Aromaticity and Magnetism. Among several indices of aromaticity, viz., bond length alteration, harmonic oscillator model of aromaticity, etc., nucleus-independent chemical shift (NICS) is often considered to be the best descriptor of aromaticity.[41] The hypothesis that a magnetic shielding tensor on a test dipole at the center of a ring can be used to quantify its magnetic property was first proposed by Elser and Haddon[42] and eventually became popular as NICS. Negative (positive) shielding tensor values are taken to indicate the presence of a diatropic (paratropic) ring current, and accordingly the system is defined as aromatic (antiaromatic).[43] The shielding tensor on any atom can be partitioned into diamagnetic and paramagnetic parts.[44] Diamagnetic shielding is considered to be the effect of opposing the magnetic field by an electron pair. Following the same analogy, any unpaired spin is likely to be aligned with the field and enhances the magnetic field at that particular point in space. This effect is manifested in the form of predominant paramagnetic shielding, which rather induces a deshielding effect.[45] This paramagnetic contribution to the shielding tensor is also known to be effected by the coupling of occupied and virtual orbitals.[44]

dx.doi.org/10.1021/ic101658a |Inorg. Chem. 2011, 50, 3234–3246

Hence, a state with a reduced HOMO−LUMO energy gap is expected to yield a higher contribution of a paramagnetic shielding tensor. Again, because the reduced HOMO−LUMO gap is generally regarded as the archetypal of antiaromaticity,[32] an antiaromatic system can be characterized by a dominant paramagnetic contribution to the shielding tensor. In this work, shielding tensors on the dummy atom as well as on the constituent atoms are computed. In this report, the isotropic shielding tensor on the dummy atom is referred to as NICS as usual,[46] and the anisotropic component of the shielding tensor on the other atoms is referred to as "$\sigma_{\parallel}$" because this component is parallel to the magnetic field and normal to the aromatic plane. During computation of this $\sigma_{\parallel}$ component and NICS, the sign convention coined by Schleyer et al. is followed.[46] According to this convention, the signs of the computed values are reversed and a negative (positive) sign is assigned for diamagnetic (paramagnetic) shielding. The choice of the gauge for the vector potential of the magnetic field is an important factor in the computation of shielding tensors.[4] This well-known gauge problem had been resolved by adopting the gauge-independent atomic orbitals method,[47] and the same method is followed in the present work to compute the shielding tensors. To find out the contribution of σ and π electrons to aromaticity, NICS has been calculated both in the center of the ring [NICS(0)],[46] and at 1 Å above the plane [NICS(1)].[48] Similar to the shielding tensor, the magnetic susceptibility tensor is also composed from diamagnetic and paramagnetic contributions.[49] The former is negative, and the latter is known to be positive. In addition to NICS, magnetic susceptibility anisotropy has been advocated as another criterion of aromaticity.[50] We report all of the three components of the susceptibility tensor (χ_{xx}, χ_{yy}, and χ_{zz}) to express the anisotropy. However, the susceptibility tensor normal to the ring (χ_{zz}), being much larger than the others, can alone represent the magnetic character of the molecule.[43]

NLO Response and Magnetism. The NLO response of an isolated molecule in an electric field F can be expressed as the coefficients of power series expansion of the total energy of the system exposed to the electric field.[51] The following expansion is written in accordance with the "B convention", where the factorial terms in the denominator originally present in the Taylor series are absorbed.[51c]

$$E = E^0 - \sum_i \mu_i F_i - \frac{1}{2}\sum_{ij} \alpha_{ij} F_i F_j - \frac{1}{3}\sum_{ijk} \beta_{ijk} F_i F_j F_k - \frac{1}{4}\sum_{ijkl} \gamma_{ijkl} F_i F_j F_k F_l - \ldots \quad (1)$$

Here E and E^0 are referred to as the energies of the perturbed and ground states; the tensors μ_i, α_{ij}, β_{ijk}, and γ_{ijkl} stand for the dipole moment, linear polarizability, and first or quadratic hyperpolarizability and second or cubic hyperpolarizability terms, respectively.[51] Generally, the field is frequency-dependent, as are the polarizability and hyperpolarizability terms. However, the centrosymmetric molecules do not have permanent dipole moments and thus their first hyperpolarizabilities become zero.[52] So, in the present work, we have computed second hyperpolarizabilities for the centrosymmetric systems. The static (frequency = 0) γ_{ijkl} is a fourth-rank tensor and is considered as the microscopic origin of third-order NLO response. The interaction between a molecular system and the electric field is usually described in terms of time-dependent perturbation theory, which becomes identical with time-independent perturbation theory in the limit of a static perturbation.[53] From eq 1, it is straightforward to express the third-order response as the fourth-order derivative of the total energy $E(F)$ with respect to the applied field in the zero-field limit.[51]

$$\gamma_{ijkl} = -\frac{1}{6}\left.\frac{\partial^4 E}{\partial F_i\, \partial F_j\, \partial F_k\, \partial F_l}\right|_{F=0} \quad (2)$$

The charge-density function $\rho(r,F)$ and the dipole moment μ of any system under perturbation caused by the electric field have an expression similar to that of eq 1.[51a,54] From these power series expansions of the charge density, dipole moment, and expression

$$\mu_i(F) = -\int \vec{r}_i \rho(r,F)\, \partial r^3 \quad (3)$$

one gets the second hyperpolarizability as

$$\gamma_{ijkl} = -\frac{1}{6}\int \vec{r}_i \rho^{(3)}_{jkl}(r)\, \partial^3 r \quad (4)$$

where $\bar{r}_i$ is the position vector with respect to the reference point on the i axis and $\rho^{(3)}_{jkl}(r) = \partial^3\rho/(\partial F_j\, \partial F_k\, \partial F_l)|_{F=0}$ is known as the second hyperpolarizability density.[55] Now, let $|S, M_s\rangle$ represent a one-dimensional spin chain with n number of sites (S and M_s are the total spin angular momentum quantum number and magnetic quantum number, respectively). In this case, each site is occupied by one unpaired electron, and then parallel and antiparallel alignment of spins on neighboring sites gives rise to two states, $|n/2, n/2\rangle$ and $|n/2, 0\rangle$, respectively, for even numbers of sites. This situation invokes the question of whether the NLO response for both situations will be the same or different. As far as eq 4 is concerned, both states having the same charge density should have the same degree of NLO response. However, following the exclusion principle, the $|n/2, 0\rangle$ state is likely to be more compact than the $|n/2, n/2\rangle$ state, and this more diffused high-spin state should give rise to a higher degree of NLO response. This conjecture is verified through the following formalism.

The longitudinal components of the integral in eq 4 can be approximated as a sum of contributions from the individual partitioned point charges on each site.[56] For instance, the second hyperpolarizability along the direction i can be expressed in the static field limit

$$\gamma_{iiii} \propto \sum_a \vec{r}_i \rho^{(3)}_a \delta(\vec{r}_i - r_{ia})|_{F_i=0} \quad (5)$$

where r_{ia} and $\rho^{(3)}_a$ are the location of site a and the so-called γ charge at that site, respectively. The quantity $\rho^{(3)}_a$ has an expression similar to that of the hyperpolarizability density

$$\rho^{(3)}_a(r) = \left.\frac{\partial^3 \rho_a}{\partial F_i^3}\right|_{F_i=0} \quad (6)$$

where ρ_a is the Mulliken point charge at site a. Now, the number of particles at site a can be obtained as the expectation value of the number operator $(\hat{n}_a)$[57]

$$\hat{n}_a = f_a^{\dagger} f_a \quad (7)$$

where $f_a^{\dagger}$ and f_a are the fermion creation and annihilation operators for site a and can be related to the spin momentum operator $\hat{S}_a^{iz}$ at that site through following Jordan−Wigner

transformation for a one-dimensional spin chain:[58]

$$\hat{S}_a^{iz} = f_a^{\dagger} f_a - \frac{1}{2} \tag{8}$$

Using eqs 6−8 and the expression

$$\hat{\rho}_a^s(\vec{r}_i) = \langle \hat{S}^{iz} \rangle^{-1} \sum_a \hat{S}_a^{iz} \delta(\vec{r}_i - r_{ia}) \tag{9}$$

where $\hat{\rho}_a^s(\vec{r}_i)$ is the spin density operator at site a,[59] and eq 5 can be written as

$$\gamma_{iiii} \propto e \sum_a \langle \hat{S}_a^{iz} \rangle \vec{r}_i \hat{\rho}'^s_a(\vec{r}_i) \tag{10}$$

where e is the charge of an electron and the expectation value of the operator $\hat{\rho}'^s_a(\vec{r}_i)$ is the third-order derivative of the Mulliken spin density with respect to the electric field at site a. The above expression defines that, although the principal cause of the second hyperpolarizability is the charge fluctuation induced by the electric field (eq 4), it may also vary for different spin configurations even if the charge density remains the same. Equation 10 delineates an enhancement of the second hyperpolarizability along a specific direction with the increased third-order derivative of the spin density at the sites oriented along that direction. To justify eq 10, in the present work we focus on the determination of longitudinal components of second hyperpolarizability γ_{iiii}, using the finite-field approach.[60] In this method, fourth-order differentiation of energy with respect to different amplitudes of the applied external electric field is used in the following expression to determine the second hyperpolarizability:[55,61]

$$\gamma_{iiii} = \{-56E_0 + 39[E(F_i) + E(-F_i)] - 12[E(2F_i) + E(-2F_i)] + [E(3F_i) + E(-3F_i)]\}/36(F_i)^4 \tag{11}$$

where $E(F_i)$ represents the total energy in the presence of static electric field F_i, applied in the i direction. To achieve numerical stability, several values of γ_{xxxx} are produced by applying minimum field strengths in the range of 0.0001−0.01 au. The field strength that produces hyperpolarizability values within the precision range of 10−100 au is regarded as numerically stable.[29] When this technique is adopted for all systems, a field strength in the range of 0.001−0.009 au is found to be numerically stable and has been employed in this work. The hyperpolarizability may have a positive or negative value depending upon the relative spatial configuration between the two hyperpolaraizability densities. The contribution of hyperpolarizability is considered positive (negative) if the direction of the arrow from a spatial point with positive (negative) hyperpolarizability density to another spatial point with negative (positive) hyperpolarizability density coincides with the positive direction of the coordinate system.[55,62] The hyperpolarizability density at each spatial point in the discretized space is deduced using the following four-point numerical differentiation formula:[55,62b]

$$\rho_{iii}^{(3)}(r) = \frac{[\rho(r, 2F_i) - \rho(r, -2F_i)] - 2[\rho(r, F_i) - \rho(r, -F_i)]}{2(F_i)^3} \tag{12}$$

where $\rho(r,F_i)$ represents the charge density at spatial point r in the presence of the field F_i. The same numerical scheme is employed on the Mulliken spin density of the system to get the third-order derivative of the spin density with respect to the electric field.

The Interplay. The preceding discussions already provide a hint that the HOMO−LUMO energy gap (ΔE_{HL}) is the factor that can play an important role to connect all three properties, viz., aromaticity, magnetism, and NLO response. The correlation of ΔE_{HL} with aromaticity becomes more prominent in the ipsocentric CTOCD-DZ formalism, where each point in a molecule is considered to be the origin of its own vector potential to tackle the gauge dependence of the magnetic-field-induced current density.[63] In this approach, the diamagnetic contribution to the orbital current density involves translational transition moments of the form $\langle \phi_v | p_\perp | \phi_o \rangle / (\varepsilon_v - \varepsilon_o)$, where ϕ_v and ϕ_o denote the virtual and occupied orbitals with corresponding energies ε_v and ε_o. The component of the electronic linear momentum in the plane perpendicular to the applied electric field is specified by $p_\perp$. Similarly, the paramagnetic part of the current density relates to the rotational transition moment of the form $\langle \phi_v | l_0 | \phi_o \rangle / (\varepsilon_v - \varepsilon_o)$, where l_0, the component of electronic angular momentum operator, is parallel to the applied magnetic field. In a state with a reduced HOMO−LUMO energy gap, the paratropic current density intensifies and the diamagnetic part of the current density is subdued for the large separation between translationally accessible states. This suggests that, in a high-spin situation, there will be a dominant paratropic ring current in the molecule.[63c] Haddon and Fuguhata demonstrated that, in annulenes, the resonance stabilization energy $\approx \Delta E_{HL}/24$, wherefrom a large ΔE_{HL} can be expected for resonance-stabilized aromatic systems.[64] Hardness, which is half of the HOMO−LUMO energy gap, is found to show a variation similar to that of aromaticity.[32] Roy et al. confirmed that increasing aromaticity causes an increase of hardness and a decrease of reactivity.[65] All of these facts point toward a direct correspondence between aromaticity and ΔE_{HL}. The same parameter ΔE_{HL} also plays an important role in the tuning of third-order NLO response. In many reports, the second hyperpolarizability is found to be inversely related with the HOMO−LUMO energy gap.[66] This HOMO−LUMO energy gap can be correlated with another parameter called the diradical character (Y_0), which is defined by the weight of a doubly excited configuration in multiconfigurational self-consistent-field theory and can also be represented by the occupation numbers of unrestricted Hartree−Fock natural orbitals.[67] It is obvious that a reduced ΔE_{HL} will effect a degenerate distribution of electrons in molecular orbitals (MOs), and in the case of precise equal distribution, one obtains $Y_0 = 1$. Thus, any connection between the diradical character and NLO response automatically indicates the relationship between ΔE_{HL} and NLO activity.[51b,68] Although the diradical character is applicable only for open-shell singlets, ΔE_{HL} can be computed for all spin states and can be regarded as a key factor in tuning the interplay among aromaticity, magnetism, and NLO response.

Among the AMASs we have chosen to establish the aforesaid interplay, the geometry of $Te_2As_2^{2-}$ is already available in CIF format and we take this form of the molecule as the ground state.[38] No such ground-state structures are available for the other systems, i.e., Al_4^{2-} and copper complexes of Al_4^{2-} and $Te_2As_2^{2-}$; hence, we optimize their structures using the unrestricted hybrid functional (UB3LYP)[69] and the Los Alamos National Laboratory double-ζ (LANL2DZ) basis set. In this basis set, the core electrons are represented by the effective core potential and the outer electrons are represented by double-ζ atomic orbitals.[70] Basically, the metals are accurately described by the LANL2DZ basis set for its ability to consider the relativistic effect.[70] This UB3LYP/LANL2DZ level of theory is invariably

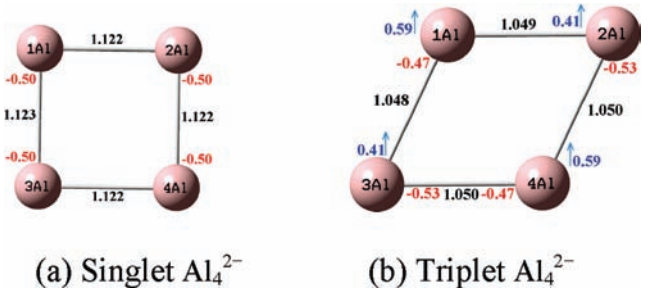

Figure 1. Charge density (red digits), spin density (blue digits; a positive value is indicated by an up-arrow), and atom−atom overlap weighted bond order (black digits).

Table 1. NICS Values (ppm) in Both Spin States of Al_4^{2-}

	singlet	triplet
NICS(0)	−27.357	4.238
NICS(1)	−23.345	1.071

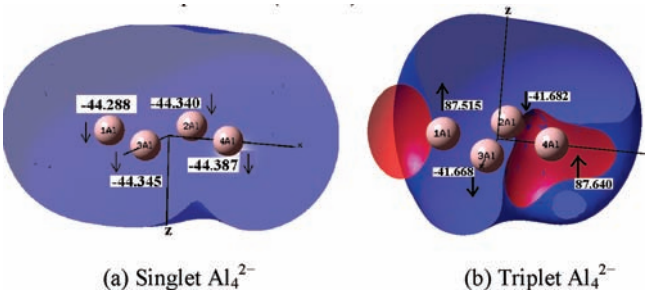

Figure 2. Diamagnetic (blue) and paramagnetic (red) contributions of $\sigma_{\parallel}$. Up-arrow and down-arrow denote the shielding and deshielding effects, respectively.

applied for each computation using *GAUSSIAN03W* suite of the quantum chemical package.[71] To judge the adequacy of the LANL2DZ results, a higher basis set, 6-311+g(3df), is employed in the case of the Al_4^{2-} system.

RESULTS AND DISCUSSION

Al_4^{2-} System. Geometry optimization of Al_4^{2-} ascertains a singlet state with D_{4h} symmetry as the ground state, while the less stable triplet state appears with D_{2h} symmetry (Figure 1). Accumulation of excess negative charges on Al2 and Al3, compared to Al1 and Al4 in the triplet state, causes this variance in the molecular structure. In a recent work, the freezing of π electrons in a parallel orientation is responsible for this distortion of the geometry in the triplet state.[72] In the present case, almost an equal majority spin density on each and individual Al atoms in the triplet state affirm this opinion (Figure 1b).

The larger negative NICS(0) value than NICS(1) suggests that Al_4^{2-} is more σ-aromatic than π-aromatic in its singlet state (Table 1). On the other hand, positive values of NICS both in and above the plane in triplet state Al_4^{2-} speak for its antiaromatic character. We find $\sigma_{\parallel}$ on each atom to have a negative value in the singlet state, indicating a diamagnetic shielding in that direction (Figure 2). In contrast, in the triplet state, Al1 and Al4, having larger spin density than Al2 and Al3, show a deshielding

Table 2. Diamagnetic and Paramagnetic Components of Susceptibility Tensors (au) in Both Spin States of Al_4^{2-} [a]

	singlet			triplet		
component	*xx*	*yy*	*zz*	*xx*	*yy*	*zz*
χ(diamagnetic)	−49.220	−49.217	−73.892	−55.427	−45.441	−76.433
χ(paramagnetic)	48.019	48.013	10.455	52.245	43.576	75.580
χ(total)		−21.947			−1.967	

[a] A magnetic field is applied along the *z* axis.

Figure 3. (a) Magnetic orbitals in triplet state Al_4^{2-}. (b) σ-Bonding situation in the fifth MO of singlet state Al_4^{2-}.

Table 3. Longitudinal Components of the Second Hyperpolarizability (in Units of 10^3 au) in Both Spin States of Al_4^{2-}

spin state	γ_{xxxx}	γ_{yyyy}	γ_{zzzz}
singlet	−18.352	−18.370	−1.958
triplet	−22.892	−23.339	−5.898

effect in the plane. A dominant contribution of the diamagnetic susceptibility appears in the singlet state, which is significantly decreased in the triplet state (Table 2).

MO analysis shows that p_y orbitals of Al1 and Al4 and p_x orbitals of Al2 and Al3 are oriented in an antibonding fashion, and hence the unpaired spins can be localized on Al atoms in the triplet state (Figure 3a). These specific orbitals are found to be in the appropriate orientation for σ bonding in the singlet state, as was found from the scrutiny of the fifth MO (Figure 3b). The seventh MO of singlet Al_4^{2-} is found to have a similar construction. Thus, bonding electrons in the singlet state become the unpaired spins in the triplet state. This statement can further be justified from the reduced atom−atom overlap weighted bond order between each Al pair in the triplet state with respect to the singlet state (Figure 1). So, it can be concluded that the bonds, maintaining σ aromaticity, are cleaved to generate radicals and aromaticity is subsequently lost.

Next, to investigate third-order NLO response, we calculate the second hyperpolarizability by applying a field strength of 0.003 au. In both spin states, the *z* component of cubic hyperpolarizability is significantly less than the other two components because the charge fluctuates mostly in the *xy* plane (Table 3). A concurrent analysis of the spin density clarifies that third-order NLO response is enhanced in the direction along which the spin density grows. This observation is in accordance with a direct correspondence between NLO response and third-order derivative of the spin density, as is apparent from eq 10. At this point, it is worth mentioning that, in the unperturbed singlet spin state of Al_4^{2-}, the Mulliken spin density is zero at each spatial point of the discretized space and so is its subsequent derivative in the presence of an electric field (Figures 1a and 4a), whereas in the triplet spin state of Al_4^{2-}, nonzero spin populations are observed on the atoms in both the unperturbed and perturbed states (Figures 1b and 4b). Hence, if an increase of

dx.doi.org/10.1021/ic101658a |*Inorg. Chem.* 2011, 50, 3234–3246

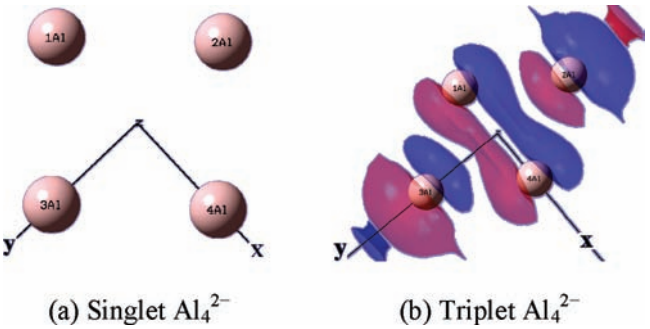

Figure 4. Third-order derivative of the spin density along the *y* axis (red and blue surfaces represent the positive and negative spin densities with isosurfaces of 100 au).

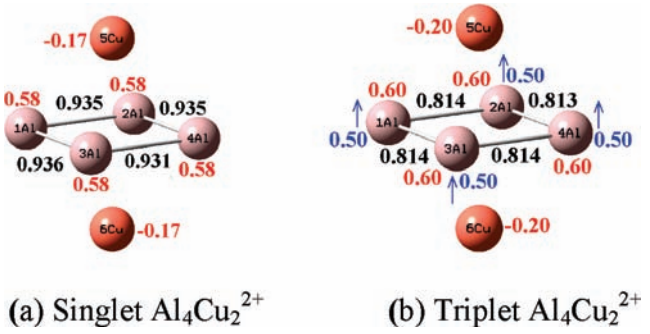

Figure 5. Charge density (red digits), spin density (blue digits; a positive value is indicated by up-arrow), and atom−atom overlap weighted bond order (black digits).

third-order NLO response from singlet to triplet states is to be accounted for on the basis of the spin density, their ground-state spin density and its third-order derivative with respect to the field give the same interpretation of the variant nonlinearity therein. In fact, in a number of references, variation of the second hyperpolarizability is explained by the ground-state charge and spin-density distribution.[29a,c,39b,51b] Relying on this observation in the other systems, the variation of NLO response is explained on the basis of ground-state spin-density distribution. Another noticeable fact is that and increase of NLO response along the *y* direction is greater than that along the *x* direction. This observation may be explained by eq 4, which suggests that more apart sites along a certain direction cause an increase in NLO response.[62a] Thus, a longer distance between Al2 and Al3 along the *y* direction causes a higher NLO response in that direction in the triplet state of Al_4^{2-} (Figure 1b).

The same set of computations with a 6-311+g(3df) basis set shows the same trend as that with the LANL2DZ level (Supporting Information), and, hence, in other systems, calculations are carried out only with this LANL2DZ basis set.

$Al_4Cu_2^{2+}$ System. In order to investigate the interaction between the metal and aromatic systems, the geometry of this complex is partially optimized, keeping the D_{4h} symmetry of aromatic Al_4^{2-} intact and sandwiching it between two Cu^{II} atoms. This optimization shows a negative charge density on Cu atoms and a slight excess of positive charge on Al atoms, which is in stark contrast with the negative charge density on the Al atoms in bare Al_4^{2-} (Figures 1 and 5). This difference in the charge density signifies charge transfer from Al to Cu atoms in

Table 4. NICS Values (ppm) in Both Spin States of $Al_4Cu_2^{2+}$

	singlet	triplet
NICS(0)	−13.582	29.128
NICS(1)	−30.779	9.261

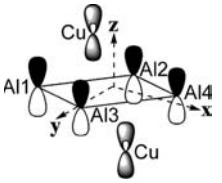

Figure 6. 22nd α-MO of singlet $Al_4Cu_2^{2+}$.

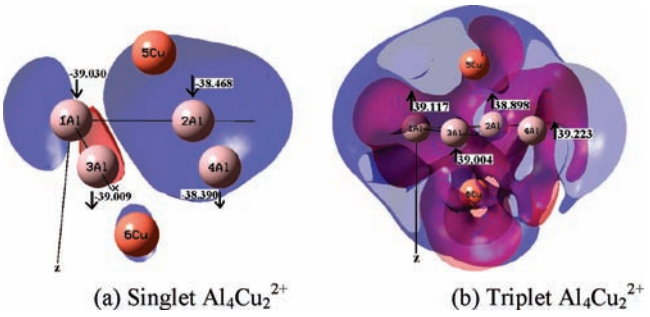

Figure 7. Diamagnetic (blue) and paramagnetic (red) contributions of $\sigma_{\parallel}$. Up-arrow and down-arrow denote the shielding and deshielding effects, respectively.

$Al_4Cu_2^{2+}$, which is also in agreement with the observation by Datta and Pati.[24,40] This charge distribution remains more or less the same in both singlet and triplet spin states (Figure 5). Charge acceptance by Cu^{II} atoms nullifies the existence of unpaired electrons in them. Consequently, the feasibility of any kind of magnetic interaction between triplet Al_4^{2-} and Cu^{II} is also annulled. Nevertheless, the presence of excess spin density on Al centers keeps the possibility of magnetic interaction open among themselves in the triplet ground state (Figure 5b).

In $Al_4Cu_2^{2+}$, computed NICS values repeat the trend of its bare analogue. However, the higher negative value of NICS(1) indicates predominant π aromaticity in the singlet state of $Al_4Cu_2^{2+}$ (Table 4), in opposition to the dominant σ aromaticity of bare Al_4^{2-}. This change in the nature of aromaticity with complexation arises from the increase of the electron density above and below the Al_4^{2-} plane due to interaction of Al orbitals with Cu orbitals (Figure 6). On the other hand, positive values of NICS in the triplet state indicate antiaromaticity in this paramagnetic species. A different magnetic nature of singlet and triplet states is also observed from the nature of the shielding tensors (Figure 7). All of the atoms are shown to produce diamagnetic shielding upon exposure to the external magnetic field in the singlet state, whereas the same set of atoms show paramagnetic shielding in the triplet state. This diamagnetic and paramagnetic nature of $Al_4Cu_2^{2+}$ in the singlet and triplet states, respectively, is further supported from their susceptibility measurement (Table 5).

From MO analysis of the triplet $Al_4Cu_2^{2+}$, sp^2 hybridized orbitals (HOs) of Al atoms appear as the magnetic orbitals

dx.doi.org/10.1021/ic101658a |*Inorg. Chem.* 2011, 50, 3234–3246

Table 5. Diamagnetic and Paramagnetic Components of Susceptibility Tensors (au) in Both Spin States of $Al_4Cu_2^{2+}$ [a]

component	singlet			triplet		
	xx	*yy*	*zz*	*xx*	*yy*	*zz*
χ(diamagnetic)	−177.569	−177.572	−52.8125	−169.396	−169.398	−53.762
χ(paramagnetic)	173.328	173.354	3.301	169.765	169.765	88.799
χ(total)		−19.324			11.926	

[a] A magnetic field is applied along the *z* axis.

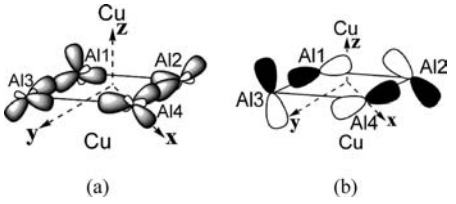

Figure 8. (a) Magnetic orbitals in triplet state $Al_4Cu_2^{2+}$. (b) 24th α-MO of singlet state $Al_4Cu_2^{2+}$.

Table 6. Longitudinal Components of Second Hyperpolarizability (in Units of 10^3 au) in Both Spin States of $Al_4Cu_2^{2+}$

spin state	γ_{xxxx}	γ_{yyyy}	γ_{zzzz}
singlet	4.174	4.619	5.178
triplet	6.985	6.968	5.442

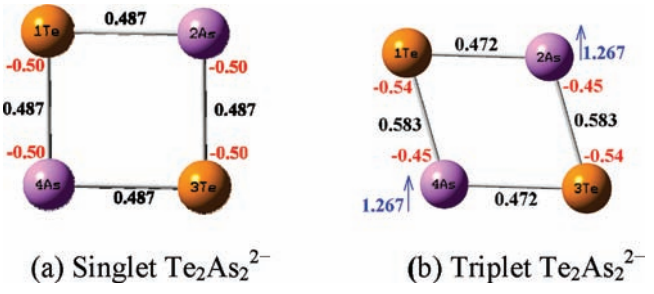

Figure 9. Charge density (red digits), spin density (blue digits; a positive value is indicated by up-arrow), and atom−atom overlap weighted bond order (black digits).

(Figure 8a). The p_y and p_x components of these sp^2 HOs in the triplet state form σ bonds among Al atoms in its singlet state, as can be seen from the schematic of 24th α-MO (Figure 8b). Lower atom−atom overlap weighted bond orders in the triplet state imply a lesser extent of electron circulation through the bonds compared to the singlet state (Figure 5). This fact and positive values of the shielding tensors in the triplet state once again complement radical generation at the expense of aromaticity.

The NLO response of this molecule, produced in the presence of 0.005 au field strength, resembles the trend observed for Al_4^{2-}. Here also, in the triplet state NLO response increases in the *x* and *y* directions along which the unpaired spins are oriented (Table 6). This observation again follows the proportionate correlation between the spin density and NLO response put in eq 10. Here, the presence of copper along the *z* component causes γ_{zzzz} to attain values not much smaller than those of other components, as was in their bare analogues.

Table 7. NICS Values (ppm) in Both Spin States of $Te_2As_2^{2-}$

	singlet	triplet
NICS(0)	55.242	−14.277
NICS(1)	44.170	−8.280

Table 8. Diamagnetic and Paramagnetic Components of Susceptibility Tensors (au) in Both Spin States of $Te_2As_2^{2-}$ [a]

component	singlet			triplet		
	xx	*yy*	*zz*	*xx*	*yy*	*zz*
χ(diamagnetic)	−75.430	−75.608	−117.559	−75.430	−75.608	−114.320
χ(paramagnetic)	50.864	50.203	113.674	50.864	50.203	87.664
χ(total)		−17.952			−21.771	

[a] A magnetic field is applied along the *z* axis.

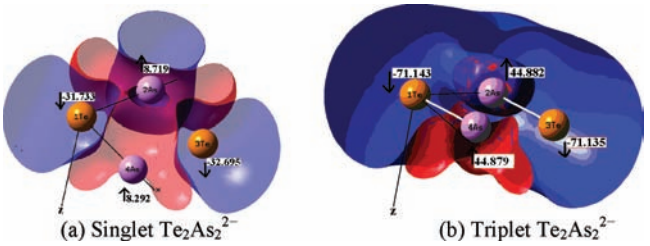

Figure 10. Diamagnetic (blue) and paramagnetic (red) contributions of $\sigma_{\parallel}$. Up-arrow and down-arrow denote the shielding and deshielding effects, respectively.

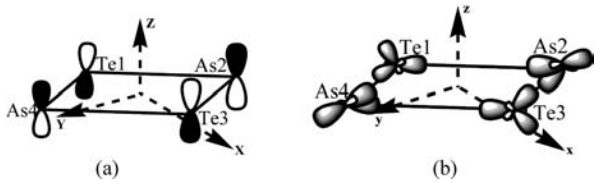

Figure 11. (a) 12th SOMO and (b) 13th SOMO in the triplet state of $Te_2As_2^{2-}$.

$Te_2As_2^{2-}$ System. The ground-state structure of this system has been retrieved from the crystallographic file of [K(18-crown-6)]$_2$[Te_2As_2].[38] The triplet state of $Te_2As_2^{2-}$ has been reported by Khanna and co-workers to be of D_{2h} symmetry (Figure 9). However, optimization of the singlet state results in a square

dx.doi.org/10.1021/ic101658a |*Inorg. Chem.* 2011, 50, 3234–3246

motif of the molecule. In this molecule, the relativistic effect becomes much more profound for the heavy Te. Hence, the effective core potential LANL2DZ becomes an appropriate choice for its ability to incorporate relativistic effects.[73] These geometries of singlet and triplet state $Te_2As_2^{2-}$ are in striking similarity with those of Al_4^{2-} (Figures 1 and 9). Once again the explanation in ref 72 is found to be applicable in the case of distortion of the geometry in the triplet state. A slight excess distribution of the charge on the Te1 and Te3 atoms may also be the reason for such distortion (Figure 9b). Urginov et al. claim that ferromagnetism is developed in $Te_2As_2^{2-}$ due to exchange interaction between localized spins on As atoms.[38] Here, we find a support to this observation from the Mulliken spin density, which shows significant spin excess on As2 and As4 atoms (Figure 9b).

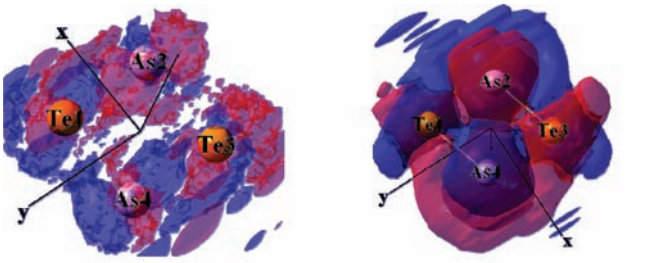

Figure 12. Hyperpolarizability density $[\rho^{(3)}_{yyy}(r)]$ distribution (red and blue surfaces represent the positive and negative γ density with isosurfaces of 30 au).

Table 9. Longitudinal Components of Second Hyperpolarizability (in Units of 10^3 au) in Both Spin States of $Te_2As_2^{2-}$

spin state	γ_{xxxx}	γ_{yyyy}	γ_{zzzz}
singlet	−4.489	−4.480	0.210
triplet	−9.265	−28.178	3.742

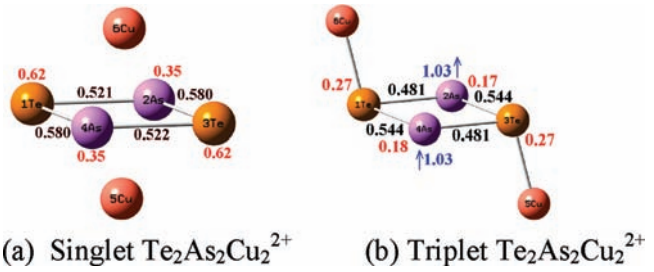

Figure 13. Charge density (red digits), spin density (blue digits; a positive value is indicated by up-arrow), and atom−atom overlap weighted bond order (black digits).

Table 10. NICS Values (ppm) in Both Spin States of $Te_2As_2Cu_2^{2+}$

	singlet	triplet
NICS(0)	−6.754	−5.104
NICS(1)	−24.614	−1.878

The high-spin state of $Te_2As_2^{2-}$ is found to be aromatic, as reflected through the negative NICS values and the susceptibility measurement (Tables 7 and 8). At the same time, a dominant paramagnetic contribution of $\sigma_{\parallel}$ on the As2 and As4 atoms in this triplet state advocates for its ferromagnetism (Figure 10). However, a positive value of NICS in the singlet state of $Te_2As_2^{2-}$ is not in parity with the susceptibility tensor, which describes diamagnetism in spite of its low negative value (Table 8). This fallacious value of the shielding tensor may emanate from the use of a small basis set like LANL2DZ. Hence, we carry out the same computation using two more different basis sets, 3-21g(d,p)[74] and SDDALL.[75] From the results, it appears that improvement upon the values of the shielding tensors can easily be performed by choosing an appropriate basis set (Supporting Information). This basis set dependence of the shielding tensor computation was addressed in a number of earlier investigations.[48,76] However, in this work to evaluate and compare the general properties, we stick to a single basis set, LANL2DZ.

The coexistence of ferromagnetism and aromaticity in the triplet state of $Te_2As_2^{2-}$ indicates that the magnetic orbitals in the triplet state are excluded from the orbitals carrying the diatropic ring current. This prediction is found to be correct through MO analysis of triplet state $Te_2As_2^{2-}$. The 12th singly occupied α-MO (SOMO) is formed from p_z orbitals of Te1, As2, Te3, and As4 (Figure 11a). The different phase signs on Te p_z and As p_z orbitals hinder them in forming π bonds, and the electrons in As p_z orbitals remain unpaired, whereas analysis of the 13th SOMO locates the unpaired spins on the As atoms in sp^2 HOs. Two lobes among the three of these HOs on each As atom find sp^2 orbitals of both the Te atoms to form σ bonds, and the remaining lobe of the sp^2 HO becomes the magnetic orbital primarily located in the As atoms (Figure 11b). From the α spin density matrix, it is clear that the density is much higher in As p_z orbitals relative to sp^2 HOs (Supporting Information); hence, the spin exchange between the electrons on the p_z orbital is more profound than that between the spins on As sp^2 HOs. Thus, it can be concluded that any change in the bonding orbitals in the *xy* plane would not affect the magnetic p_z orbital. However, Te1−As4 and As2−Te3 pairs surprisingly show a significant decrease in the bond order in the singlet state (Figure 9). To explain this anomaly, Figure 11b is recalled. This 13th MO of the triplet state shows a strong overlap between Te1−As4 and As2−Te3 pairs, whereas this particular bonding situation is

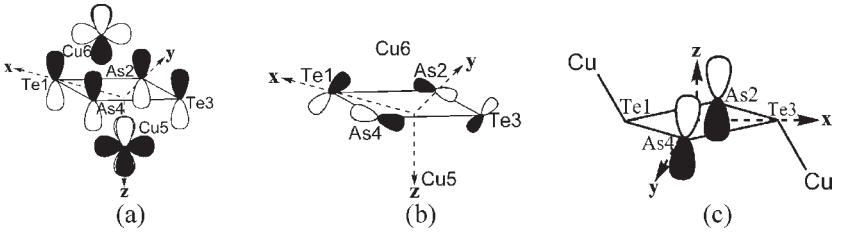

Figure 14. (a) 13th α-MO of singlet state $Te_2As_2Cu_2^{2+}$. (b) 16th α-MO in $Te_2As_2Cu_2^{2+}$. (c) Magnetic orbital in triplet state $Te_2As_2Cu_2^{2+}$.

dx.doi.org/10.1021/ic101658a |*Inorg. Chem.* 2011, 50, 3234–3246

found missing between the same pairs among all of the MOs of the singlet state. This absence of overlap between neighboring atomic orbitals, in fact, causes a cessation in the flow of electrons, and consequently the singlet state tends toward antiaromaticity. This fact of reducing aromaticity from the triplet to singlet state is prominent from a comparison of the susceptibilities therein (Table 8).

The second hyperpolarizability is computed by applying a finite field of 0.0015 au. During this computation, the coordinate axes are set through the middle of the bond between Te and As (Figure 12), and hence we cannot relate the growing spin density on the atoms and NLO response as before. Nevertheless, it follows from Table 9 that the increase in NLO response in the y direction is 1 order of magnitude higher than that along the x direction. This can be explained by eq 4, which predicts an increase in NLO behavior with increased second hyperpolarizability density. From Figure 9, it is evident that the atom−atom weighted bond order between Te1−As4 and As2−Te3 pairs increases in the triplet state compared to the singlet state owing to the formation of σ bonds. The σ bonding causes more accumulation of the electron density between the atoms, and this amplified charge density gives rise to a significant enhancement in the cubic hyperpolarizability in the y direction (Table 9). The hyperpolarizability density plot along the y direction also supports this fact (Figure 12), and hence it can be concluded that the unperturbed charge density and second hyperpolarizability density lead to the similar interpretations of NLO response.

$Te_2As_2Cu_2^{2+}$ System. The geometry of this molecule is partially optimized, keeping the aromaticity of triplet state $Te_2As_2^{2-}$ intact and sandwiching it between two Cu^{II} atoms. In the triplet state, the Cu5 and Cu6 atoms are found to form strong bonds with the Te3 and Te1 atoms, respectively, whereas in the singlet state, the Cu atoms remain equidistant from all of the atoms in the $Te_2As_2^{2-}$ plane (Figure 13). With this variation in the structure, the triplet state appears to be the ground state.

The larger negative NICS(1) value signifies a prevailing π aromaticity in the singlet state of $Te_2As_2Cu_2^{2+}$ (Table 10), which may be attributed to the interaction of orbitals belonging to Te and As with that of Cu (Figure 14a). This NICS(1) value is significantly decreased in the triplet state (Table 10), owing to the bonding of Cu atoms with Te atoms only (Figure 13b). Because of this bonding pattern, the charge density above and below the plane loses its symmetry, leading to a loss of the diatropic ring current through the π bond and subsequent π aromaticity. This decreases in π-electron circulation finds its evidence in a decrease in athe tom−atom weighted bond order while going from the singlet to triplet state (Figure 13). However, in spite of a considerable decrease in the π aromaticity, the σ aromaticity remains almost unaltered with a change in spin multiplicity because of the possibility of σ-bonding interaction in both spin states. The orbital orientation, as is visible from the 16th MO, creates the required zone for itinerancy of electrons to induce σ aromaticity in both spin states (Figure 14b). Moreover, the σ aromaticity in the xy plane does not disturb the magnetic orbitals on As atoms oriented along the z direction (Figure 14c).

The bonding of Cu atoms with Te atoms only causes accumulation of excess spin on the As2 and As4 atoms, as can be seen from the HOMO of the triplet state (Figure 14c). The growing radical character of As atoms in the triplet state is well reflected through a dominant paramagnetic contribution of the $\sigma_{\parallel}$ value. The different nature of the shielding tensors in low and high spin states is distinct from Figure 15. However, the sign of total susceptibility and NICS remain negative in both spin states, indicating retention of the aromatic character (Tables 10 and 11).

The hyperpolarizabilities are calculated in the numerically stable field of strength 0.002 au. The hyperpolarizability exaltation along the z direction in the copper complex in comparison with $Te_2As_2^{2-}$ can be attributed to the presence of copper in that direction (Table 12). Following the previous trends, cubic hyperpolarizability along the y direction is increased with an increase in the spin density on As atoms in the triplet state. The intense increase in γ_{xxxx} in the triplet state can be explained by eq 4, according to which an increase in the second hyperpolarizability density should bring about an increase in the third-order nonlinearity. In the triplet state, the x axis is slightly distorted from its position in the singlet state and passes through the newly formed bonds between Te and As atoms (Figure 16). Consequently, more electron density is available along that direction in the triplet state than in the singlet state, which causes this

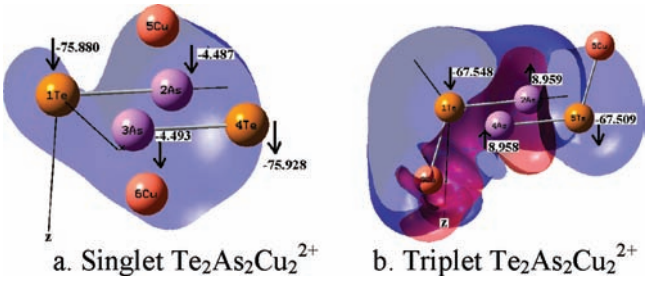

Figure 15. Diamagnetic (blue) and paramagnetic (red) contributions of $\sigma_{\parallel}$. Up-arrow and down-arrow denote the shielding and deshielding effects, respectively.

Table 12. Longitudinal Components of Second Hyperpolarizability (in Units of 10^3 au) in Both Spin States of $Te_2As_2Cu_2^{2+}$

spin state	γ_{xxxx}	γ_{yyyy}	γ_{zzzz}
singlet	1.802	1.524	5.960
triplet	58.493	4.248	8.974

Table 11. Diamagnetic and Paramagnetic Components of Susceptibility Tensors (au) in Both Spin States of $Te_2As_2Cu_2^{2+}$[a]

	singlet			triplet		
component	xx	yy	zz	xx	yy	zz
χ(diamagnetic)	−193.149	−188.246	−100.815	−342.479	−368.498	−500.822
χ(paramagnetic)	177.943	180.592	71.867	320.957	349.125	480.112
χ(total)		−17.270			−20.535	

[a] A magnetic field is applied along the z direction.

dx.doi.org/10.1021/ic101658a |Inorg. Chem. 2011, 50, 3234–3246

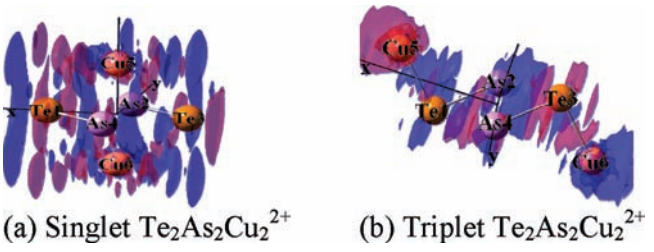

Figure 16. Hyperpolarizability density $[\rho^{(3)}_{xxx}(r)]$ distribution (red and blue surfaces represent the positive and negative γ density with isosurfaces of 100 au).

Table 13. HOMO−LUMO Energy Gap (ΔE_{HL}) of All of the Compounds under Investigation

system	spin multiplicity	ΔE_{HL} (au)
Al_4^{2-}	1	0.086
	3	0.006
$Al_4Cu_2^{2+}$	1	0.040
	3	0.018
$Te_2As_2^{2-}$	1	0.033
	3	0.005
$Te_2As_2Cu_2^{2+}$	1	0.070
	3	0.019

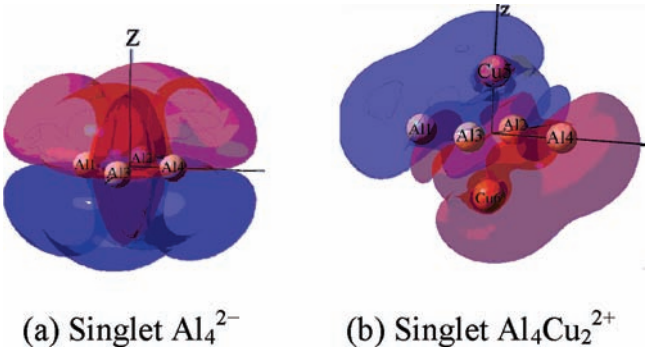

Figure 17. Hyperpolarizability density $[\rho^{(3)}_{zzz}(r)]$ distribution (red and blue surfaces represent the positive and negative γ- density with isosurfaces of 100 au).

noticeable increase in the hyperpolarizability density in that direction (Figure 16).

CONCLUSIONS

The AMASs investigated in this work are found to have multiple aromaticity irrespective of the spin states. On the basis of their change in aromaticity with the spin state, they can be categorized in two distinct classes. At one end, Al_4^{2-} and $Al_4Cu_2^{2+}$, which are aromatic in the singlet state, behave as antiaromatic in their triplet state. This swap of aromaticity is found to be associated with the weakening of σ bonds while going from the singlet to triplet state. A similar type of alternation in the aromaticity pattern vis-á-vis bond-stretch isomerism was noticed in X_3^{2-} (X = Be, Mg, and Ca) and their sodium complexes, where in a few cases swapping of the frontier MOs was observed.[77] Thus, it can be surmised that the orbitals used to maintain the diatropic ring current in the singlet state turn into magnetic orbitals in the triplet state, and this, in turn, establishes an antagonistic relationship between the aromaticity and spin excess in the first type of AMAS. On the contrary, in $Te_2As_2^{2-}$ and $Te_2As_2Cu_2^{2+}$, one can trace the simultaneous existence of aromaticity and high spin state. This situation arises because the magnetic orbitals, containing spin excess, and the orbitals required for the diatropic ring current leading to aromaticity are not the same. However, in the singlet state, they show a tendency toward antiaromaticity, which becomes apparent from a decrease in the negative value of susceptibility. This propensity toward antiaromaticity in the singlet state can be explained by the simple electron count rule. For all of the systems under investigation, the atoms with excess spin density are found to be associated with an enhanced paramagnetic contribution of the shielding tensor. Moreover, this overriding paramagnetic contribution of $\sigma_{\parallel}$ is found in the states that are predominantly antiaromatic. Both this dominant paramagnetic $\sigma_{\parallel}$ and antiaromaticity are observed in the higher spin states. This can be well explained from the relative lowering of the HOMO−LUMO energy gap in these states (Table 13). This reduced ΔE_{HL} facilitates the mixing of HOMO and LUMO, which, in turn, gives rise to the antiaromaticity and exaltation of the paramagnetic shielding tensor.

A significant number of works highlight the variance of NLO response with a change in the spin multiplicity.[29,78] A detailed study of the NLO behavior in open-shell systems also displays the dependence of NLO response on the nature of the spin.[79] We rationalize these observations by correlating NLO response with the spin density of any system. In a recent work, it has been shown that the inherent magnetism of any material is dependent on the spin density at the magnetic sites.[80] Hence, the correlation between the spin density and NLO response enables one to relate magnetism with the NLO behavior. From computation of the second hyperpolarizability, an increase in NLO response is observed in the systems with excess spin density in them, as expected from eq 10. In the copper complexes of Al_4^{2-} and $Te_2As_2^{2-}$, the presence of copper along the z direction causes an increase of the charge density and subsequent exaltation in γ_{zzzz} in that direction. However, because NLO response is related with the third-order derivative of the electron density with respect to the electric field (eq 4), it becomes important to check the variation of the hyperpolarizability density. From Figures 12 and 16, it has already been found that the ground-state charge density distribution explains the variation of NLO response in the same way as does the hyperpolarizability density. This trend is also found to be true for the γ_{zzzz} components. The increase of the hyperpolarizability density along the z direction of $Al_4Cu_2^{2+}$ compared to Al_4^{2-} is similar to their ground-state charge distributions, and hence the ground-state charge density becomes equally meaningful as the second hyperpolarizability density in explaining the increase in the γ_{zzzz} component. Interestingly, the γ components are also changed in sign upon the introduction of Cu^{II} atoms into planar Al_4^{2-} and $Te_2As_2^{2-}$ structures. This fact can be explained by comparing the corresponding hyperpolarizability density plots. It is distinct from Figure 17 that the relative spatial orientation of the hyperpolarizability densities is changed along the z direction, causing inversion of the sign in the γ_{zzzz}component from Al_4^{2-} to $Al_4Cu_2^{2+}$ (Tables 3 and 6). Similar hyperpolarizability density plots are observed in all other cases where such inversion of the

dx.doi.org/10.1021/ic101658a |Inorg. Chem. 2011, 50, 3234–3246

sign in the γ component occurs. This spatial inversion of the positive and negative γ density may be attributed to charge transfer between copper and the metal ring.[24,40]

To summarize, in the investigated all-metal aromatic clusters, the properties, viz., aromaticity, magnetism, and NLO response, are found to be correlated. The reason for such interplay among the properties underlies basically in the tuning of the HOMO−LUMO energy gap. Because parameter ΔE_{HL} also affects the hardness and hence the reactivity of any system, higher reactivity of any system can be associated with antiaromaticity[81] as well as high NLO response. Nevertheless, from analysis of how different parameters like the charge density, spin density, or HOMO−LUMO energy gap can control the interplay, it becomes obvious that this interplay is system-independent and should have subsistence beyond the domain of all-metal aromatic clusters. The simultaneous existence of different important properties in AMASs certainly provides a boost in the quest of multifunctional materials. The increase in NLO response with spin density may stimulate the idea of a new class of "spin-enhanced NLO systems".[29c,36b] Such systems with large NLO response can be cast as the building block of optoelectronic devices for telecommunication and information storage, optical switches for signal processing, sensors for biological or chemical processes, and so on.[82]

■ ASSOCIATED CONTENT

Supporting Information. MOs (generated from the checkpoint file of MO output) describing Figures 3, 6, 8, 11, and 14 in the text (Figures S1−S10), contributions of different p orbitals in composing the magnetic orbital in $Te_2As_2^{2-}$ (Table S1), NICS calculated for $Te_2As_2^{2-}$ using other basis sets (Table S2), optimized coordinates of all four systems in their singlet and triplet states (Tables S3−S10), different properties of Al_4^{2-} computed at the UB3LYP/6-311+g(3df) level of theory (Figures S11 and S12 and Tables S11−S13), and complete ref 71. This material is available free of charge via the Internet at http://pubs.acs.org.

■ AUTHOR INFORMATION

Corresponding Author
*E-mail: anirbanmisra@yahoo.com.

■ ACKNOWLEDGMENT

We sincerely thank the Department of Science and Technology, India, for financial support.

■ REFERENCES

(1) (a) Li, X.; Kuznetsov, A. E.; Zhang, H. F.; Boldyrev, A. I.; Wang, L. S. *Science* **2001**, *291*, 859. (b) Ritter, S. K. *Chem. Eng. News* **2001**, *79*, 39. (c) Boldyrev, A. I.; Wang, L. S. *Chem. Rev.* **2005**, *105*, 3716.

(2) (a) Li, X.; Zhang, H. F.; Wang, L. S.; Kuznetsov, A. E.; Cannon, N. A.; Boldyrev, A. I. *Angew. Chem., Int. Ed.* **2001**, *40*, 1867. (b) Kuznetsov, A. E.; Boldyrev, A. I.; Li, X.; Wang, L. S. *J. Am. Chem. Soc.* **2001**, *123*, 8825.

(3) (a) Twamley, B.; Power, P. P. *Angew. Chem., Int. Ed.* **2000**, *39*, 3500. (b) Cisar, A.; Corbett, J. D. *Inorg. Chem.* **1977**, *16*, 2482. (c) Critchlow, S. C.; Corbett, J. D. *Inorg. Chem.* **1984**, *23*, 770. (d) Tuononen, H. M.; Suontamo, R.; Valkonen, J.; Laitinen, R. S. *J. Phys. Chem. A* **2004**, *108*, 5670.

(4) (a) Todorov, I.; Sevov, S. C. *Inorg. Chem.* **2004**, *43*, 6490. (b) Todorov, I.; Sevov, S. C. *Inorg. Chem.* **2005**, *44*, 5361.

(5) (a) Gillespie, R. J.; Barr, J.; Kapoor, R.; Malhotra, K. C. *Can. J. Chem.* **1968**, *46*, 149. (b) Gillespie, R. J.; Barr, J.; Crump, D. B.; Kapoor, R.; Ummat, P. K. *Can. J. Chem.* **1968**, *46*, 3607. (c) Barr, J.; Gillespie, R. J.; Kapoor, R.; Pez, G. P. *J. Am. Chem. Soc.* **1968**, *90*, 6855. (d) Couch, T. W.; Lokken, D. A.; Corbett, J. D. *Inorg. Chem.* **1972**, *11*, 357.(e) Burford, N.; Passmore, J.; Sanders, J. C. P. In *From Atoms to Polymers. Isoelectronic Analogies*; Liebman, J. F., Greenburg, A., Eds.; VCH: New York, 1989; pp 53−108.

(6) (a) Li, X.; Wang, X. B.; Wang, L. S. *Phys. Rev. Lett.* **1998**, *81*, 1909. (b) Wu, H.; Li, X.; Wang, X. B.; Ding, C. F.; Wang, L. S. *J. Chem. Phys.* **1998**, *109*, 449. (c) Baeck, K. K.; Bartlett, R. J. *J. Chem. Phys.* **1998**, *109*, 1334. (d) Kuznetsov, A. E.; Boldyrev, A. I. *Struct. Chem.* **2002**, *13*, 141.

(7) Kuznetsov, A. E.; Boldyrev, A. I.; Zhai, H. J.; Li, X.; Wang, L. S. *J. Am. Chem. Soc.* **2002**, *124*, 11791.

(8) (a) Nielsen, J. W.; Baenziger, N. C. *Acta Crystallogr.* **1954**, *7*, 277. (b) Corbett, J. D. *Inorg. Nucl. Chem. Lett.* **1969**, *5*, 81. (c) Kuznetsov, A. E.; Corbett, J. D.; Wang, L. S.; Boldyrev, A. I. *Angew. Chem., Int. Ed.* **2001**, *40*, 3369.

(9) (a) Gausa, M.; Kaschner, R.; Lutz, H. O.; Seifert, G.; Broer, K. H. M. *Chem. Phys. Lett.* **1994**, *230*, 99. (b) Gausa, M.; Kaschner, R.; Seifert, G.; Faehrmann, J. H.; Lutz, H. O.; Meiwes, K. H. B. *J. Chem. Phys.* **1996**, *104*, 9719. (c) Zhai, H. J.; Wang, L. S.; Kuznetsov, A. E.; Boldyrev, A. I. *J. Phys. Chem. A* **2002**, *106*, 5600.

(10) Tanaka, H.; Neukermans, S.; Janssens, E.; Silverans, R. E.; Lievens, P. *J. Am. Chem. Soc.* **2003**, *125*, 2862.

(11) Alexandrova, A. N.; Boldyrev, A. I.; Zhai, H. J.; Wang, L. S. *J. Phys. Chem. A* **2005**, *109*, 562.

(12) Wannere, C. S.; Corminboeuf, C.; Wang, Z.-X.; Wodrich, M. D.; King, R. B.; Schleyer, P. v. R. *J. Am. Chem. Soc.* **2005**, *127*, 5701.

(13) Lein, M.; Frunzke, J.; Frenking, G. *Angew. Chem., Int. Ed.* **2003**, *42*, 1303.

(14) Chattaraj, P. K.; Roy, D. R.; Elango, M.; Subramanian, V. *J. Phys. Chem. A* **2005**, *109*, 9590.

(15) (a) Mercero, J. M.; Ugalde, J. M. *J. Am. Chem. Soc.* **2004**, *126*, 3380. (b) Mercero, J. M.; Formoso, E.; Matxain, J. M.; Eriksson, L. A.; Ugalde, J. M. *Chem.—Eur. J.* **2006**, *12*, 4495.

(16) Wei, L. Z.; Yuan, Z. C.; Sheng, W. W.; Ping, C. L. *Chinese J. Struct. Chem.* **2008**, *27*, 1097.

(17) Yang, M.; Ding, Y.; Sun, C. *Chem.—Eur. J.* **2007**, *13*, 2546.

(18) (a) Garratt, P. J. *Aromaticity*; McGraw-Hill: London, 1971. (b) Krygowski, T. M.; Cyranski, M. K.; Czarnocki, Z.; Hafelinger, G.; Katritzky, A. R. *Tetrahedron* **2000**, *56*, 1783. (c) Lloyd, D. *J. Chem. Inf. Comput. Sci.* **1996**, *36*, 442. (d) Schleyer, P. v. R.; Jiao, H. *Pure Appl. Chem.* **1996**, *68*, 209.

(19) (a) Minkin, V. I.; Glukhovtsev, M. N.; Simkin, B. Y. *Aromaticity and Antiaromaticity, Electronic and Structural Aspects*; John Wiley and Sons: New York, 1994. (b) Mills, N. S.; Malandra, J. L.; Burns, E. E.; Green, A.; Gibbs, J.; Unruh, K. E.; Kadlecek, D. E.; Lowery, J. A. *J. Organomet. Chem.* **1998**, *62*, 9318. (c) Mills, N. S.; Burns, E. E.; Hodges, J.; Gibbs, J.; Esparza, E.; Malandra, J. L.; Koch, J. *J. Organomet. Chem.* **1998**, *63*, 3017. (d) Alkorta, I.; Rozas, I.; Elguero, J. *Tetrahedron* **2001**, *57*, 6043.

(20) (a) Fowler, P. W.; Havenith, R. W. A.; Steiner, E. *Chem. Phys. Lett.* **2001**, *342*, 85. (b) Fowler, P. W.; Havenith, R. W. A.; Steiner, E. *Chem. Phys. Lett.* **2002**, *359*, 530.

(21) Chen, Z.; Corminboeuf, C.; Heine, T.; Bohmann, J.; Schleyer, P. v. R. *J. Am. Chem. Soc.* **2003**, *125*, 13930.

(22) Havenith, R. W. A.; Fowler, P. W.; Steiner, E.; Shetty, S.; Kanhere, D. G.; Pal, S. *Phys. Chem. Chem. Phys.* **2004**, *6*, 285.

(23) Kuznetsov, A. E.; Birch, K. A.; Boldyrev, A. I.; Li, X.; Zhai, J. H.; Wang, L. S. *Science* **2003**, *300*, 622.

(24) (a) Datta, A.; Pati, S. K. *J. Phys. Chem. A* **2004**, *108*, 9527. (b) Datta, A.; Pati, S. K. *Chem. Commun.* **2005**, 5032.

(25) (a) Fang, L.; Yang, G. C.; Qiu, Y. Q.; Su, Z. M. *Theor. Chem. Acc.* **2009**, *119*, 329. (b) Sen, S.; Seal, P.; Chakrabarty, S. *Phys. Rev. B* **2007**, *76*, 115414.

(26) Shetty, S.; Kanhare, D. G.; Pal, S. *J. Phys. Chem. A* **2004**, *108*, 628.
(27) (a) Li, D.; Marks, T. J.; Ratner, M. A. *J. Phys. Chem.* **1992**, *96*, 4325. (b) Ramasesha, S.; Soos, Z. G. *Chem. Phys. Lett.* **1988**, *158*, 171.
(28) (a) Bendikov, M.; Duong, H. M.; Starkey, K.; Houk, K. N.; Carter, E. A.; Wudl, F. *J. Am. Chem. Soc.* **2004**, *126*, 7416. (b) Malloci, G.; Mulas, G.; Cappellini, G.; Joblin, C. *Chem. Phys.* **2007**, *340*, 43. (c) Reddy, A. R.; Fridman, M. G.; Benidikov, M. *J. Org. Chem.* **2007**, *72*, 51. (d) Clar, E. *The Aromatic Sextet*; John Wiley and Sons: New York, 1970. (e) Bhattacharya, D.; Shil, S.; Misra, A.; Klein, D. J. *Theor. Chem. Acc.* **2010**, *127*, 57.
(29) (a) Nakano, M.; Nagai, H.; Fukui, H.; Yoneda, K.; Kishi, R.; Takahashi, H.; Shimizu, A.; Kubo, T.; Kamada, K.; Ohta, K.; Champagne, B.; Botek, E. *Chem. Phys. Lett.* **2008**, *467*, 120. (b) Nakano, M.; Kishi, R.; Nitta, T.; Kubo, T.; Nakasaji, K.; Kamada, K.; Ohta, K.; Champagne, B.; Botek, E.; Yamaguchi, K. *J. Phys. Chem. A* **2005**, *109*, 885. (c) Nakano, M.; Nitta, T.; Yamaguchi, K.; Champagne, B.; Botek, E. *J. Phys. Chem. A* **2004**, *108*, 4105.
(30) Avci, D.; Comert, H.; Atalay, Y. *J. Mol. Model.* **2008**, *14*, 161.
(31) (a) Minsky, A.; Meyer, A. Y.; Poupku, R.; Rabinovitz, M. *J. Am. Chem. Soc.* **1983**, *105*, 8.(b) Dewar, M. J. S. *Angew. Chem.* **1971**, *10*, 761; 83, 859. (c) Volhard, K. P. C.; Yee, L. S. *J. Am. Chem. Soc.* **1983**, *105*, 7512. (d) Willner, I.; Rabinovitz, M. *J. Org. Chem.* **1980**, *45*, 1628. (e) Cohen, Y.; Klein, J.; Rabinovitz, M. *J. Chem. Soc., Chem. Commun.* **1986**, 1071. (f) Cohen, Y.; Roelofs, N. H.; Reinhard, G.; Scott, L. T.; Rabinovitz, M. *J. Org. Chem.* **1987**, *52*, 4207. (g) Budzelar, P. H. M.; Cremer, D.; Wallasch, M.; Wurthwein, E. U.; Schleier, P. v. R. *J. Am. Chem. Soc.* **1987**, *109*, 6290.
(32) (a) Carey, F. A.; Sundberg, R. J. *Advanced Organic Chemistry: Structure and Mechanisms*; Springer: Berlin, 2007. (b) Zhou, Z.; Navangul, H. V. *J. Phys. Org. Chem.* **1990**, *3*, 784. (c) Chamizo, J. A.; Morgado, J.; Sosa, O. *Organometallics* **1993**, *12*, 5005. (d) Bird, C. W. *Tetrahedron* **1997**, *53*, 2497.
(33) Lamere, J. F.; Malfant, I.; Saquet, A. S.; Lacroix, P. G. *Chem. Mater.* **2007**, *19*, 805.
(34) (a) Nakano, M.; Kishi, R.; Ohta, S.; Takahashi, H.; Kubo, T.; Kamada, K.; Ohta, K.; Botek, E.; Champagne, B. *Phys. Rev. Lett.* **2007**, *99*, 033001. (b) Nakano, M.; Yoneda, K.; Kishi, R.; Takahashi, H.; Kubo, T.; Kamada, K.; Ohta, K.; Botek, E.; Champagne, B. *J. Chem. Phys.* **2009**, *131*, 114316.
(35) (a) Goze, F.; Laukhin, V. N.; Brossard, L.; Audouard, A.; Ulmet, J. P.; Askenazy, S.; Nalto, T.; Kobayashi, H.; Kobayashi, M.; Cassoux, P. *Europhys. Lett.* **1994**, *28*, 427. (b) Kurmoo, M.; Graham, A. W.; Day, P.; Coles, S. J.; Hursthouse, M. B.; Caulfield, J. L.; Singleton, J.; Pratt, F. L.; Hayes, W.; Ducasse, L.; Guionneau, P. *J. Am. Chem. Soc.* **1995**, *117*, 12209.
(36) (a) Sutter, K.; Hulliger, J.; Gunter, P. *Solid State Commun.* **1990**, *74*, 867. (b) Lacroix, P. G.; Nakatani, K. *Adv. Mater.* **1997**, *9*, 1105.
(37) (a) Clément, R.; Lacroix, P. G.; O'Hare, D.; Evans, J. *Adv. Mater.* **1994**, *6*, 794. (b) Lacroix, P. G.; Clément, R.; Nakatani, K.; Zyss, J.; Ledoux, I. *Science* **1994**, *263*, 658. (c) Bernard, S.; Yu, P.; Coradin, T.; Rivière, E.; Nakatani, K.; Clément, R. *Adv. Mater.* **1997**, *9*, 981.
(38) Urginov, A.; Sen, A.; Reber, A. C.; Qian, M.; Khanna, S. N. *J. Am. Chem. Soc.* **2008**, *130*, 782.
(39) (a) Levine, B. F. *Chem. Phys. Lett.* **1976**, *37*, 516. (b) Bella, S. D.; Fragala, I. L.; Ratner, M. A.; Marks, T. J. *J. Am. Chem. Soc.* **1993**, *115*, 682. (c) Li, Z. J.; Wang, F. F.; Xu, H. L; Huang, X. R.; Wu, D.; Chen, W.; Yu, G. T.; Gu, F. L.; Aoki, Y. *Phys. Chem. Chem. Phys.* **2009**, *11*, 402.
(40) Datta, A.; Pati, S. *J. Am. Chem. Soc.* **2005**, *127*, 3496.
(41) (a) Cyranski, M. K.; Krygowski, T. M.; Katritzky, A. R.; Schleyer, P. v. R. *J. Org. Chem.* **2002**, *67*, 1333. (b) Portella, G.; Poater, J.; Sola, M. *J. Phys. Org. Chem.* **2005**, *18*, 785.
(42) Elser, V.; Haddon, R. C. *Nature (London)* **1987**, *325*, 792.
(43) Lazzeretti, P. *Phys. Chem. Chem. Phys.* **2004**, *6*, 217.
(44) (a) Schreckenbach, G.; Ziegler, T. *J. Phys. Chem.* **1995**, *99*, 606. (b) Morales, Y. R.; Schreckenbach, G.; Ziegler, T. *J. Phys. Chem.* **1996**, *100*, 3359.
(45) (a) Koo, I. S.; Ali, D.; Yang, K.; Park, Y.; Wardlaw, D. M.; Buncel, E. *Bull. Korean Chem. Soc.* **2008**, *29*, 2252. (b) Casabianca, L. B.; De Dios, A. C. *J. Chem. Phys.* **2008**, *128*, 052201.
(46) Schleyer, P. v. R.; Maerker, C.; Dransfeld, A.; Jiao, H.; Hommes, N. J. R. V. E. *J. Am. Chem. Soc.* **1996**, *118*, 6317.
(47) (a) Ditchfield, R. *Mol. Phys.* **1974**, *27*, 789. (b) Fukui, H. *Magn. Reson. Rev.* **1987**, *11*, 205. (c) Freidrich, K.; Seifert, G.; Grossmann, G. *Z. Phys. D* **1990**, *17*, 45.(d) Malkin, V. G.; Malkina, O. L.; Erikson, L. A.; Salahub, D. R. In *Density Functional Calculations; Vol. 1 of theoretical and computational chemistry*; Politzer, P., Seminario, J. M., Eds.; Elsevier: Amsterdam, The Netherlands, 1995.
(48) (a) Schleyer, P. v. R.; Jiao, H.; Hommes, N. J. R. V. E.; Malkin, V. G.; Malkina, O. *J. Am. Chem. Soc.* **1997**, *119*, 12669. (b) Schleyer, P. v. R.; Manoharan, M.; Wang, Z. X.; Kiran, B.; Jiao, H.; Pachta, R.; Hommes, N. J. R. V. E. *Org. Lett.* **2001**, *3*, 2465.
(49) Vleck, J. H. V. *Electric and Magnetic Susceptibility*; Oxford University Press: London, 1932.
(50) (a) Benson, R. C.; Flygare, W. H. *J. Am. Chem. Soc.* **1970**, *92*, 7523. (b) Schmalz, T. G.; Norris, C. L.; Flygare, W. H. *J. Am. Chem. Soc.* **1973**, *95*, 7961. (c) Schmalz, T. G.; Gierke, T. D.; Beak, P.; Flygare, W. H. *Tetrahedron Lett.* **1974**, *33*, 2885. (d) Palmer, M. H.; Findlay, R. H. *Tetrahedron Lett.* **1974**, *33*, 253. (e) Hutter, D. H.; Flygare, W. H. *Top. Curr. Chem.* **1976**, *63*, 89. (f) Fleischer, U.; Kutzelnigg, W.; Lazzeretti, P.; Miihlenkamp, V. *J. Am. Chem. Soc.* **1994**, *116*, 5298.
(51) (a) Yamada, S.; Nakano, M.; Yamaguchi, K. *Int. J. Quantum Chem.* **1999**, *71*, 329. (b) Ohta, S.; Nakano, M.; Kubo, T.; Kamada, K.; Ohta, K.; Kishi, R.; Nakagawa, N.; Champagne, B.; Botek, E.; Takebe, A.; Umezaki, S.; Natu, M.; Takahashi, H.; Furukawa, S.; Morita, Y.; Nakasuji, K.; Yamaguchi, K. *J. Phys. Chem. A* **2007**, *111*, 3633. (c) Willetts, A.; Rice, J. E.; Burland, D. M.; Shelton, D. P. *J. Chem. Phys.* **1992**, *97*, 7590.
(52) (a) Buckingham, A. D. *Philos. Trans. R. Soc., A* **1979**, *293*, 239. (b) Kanis, D. R.; Wong, J. S.; Marks, T. J.; Ratner, M. A.; Zabrodsky, H.; Keinan, S.; Avnir, D. *J. Phys. Chem.* **1995**, *99*, 11061.
(53) Olsen, J.; Jorgensen, P. *J. Chem. Phys.* **1985**, *82*, 3235.
(54) (a) Chopra, P.; Carlacci, L.; King, H.; Prasad, P. N. *J. Phys. Chem.* **1989**, *93*, 7120. (b) Nakano, M.; Yamada, S.; Takahata, M.; Yamaguchi, K. *J. Phys. Chem. A* **2003**, *107*, 4157and references cited therein..
(55) Nakano, M.; Shigemoto, I.; Yamada, S.; Yamaguchi, K. *J. Chem. Phys.* **1995**, *103*, 4175.
(56) An, Z.; Wong, K. Y. *J. Chem. Phys.* **2003**, *119*, 1204.
(57) Kittel, C. *Quantum Theory of Solids*; John Wiley & Sons, Inc.: New York, 1987.
(58) Jordan, P.; Wigner, E. P. *Z. Phys.* **1928**, *47*, 631.
(59) (a) Nakatsuji, H.; Hirao, K. *J. Chem. Phys.* **1978**, *68*, 4279. (b) Kollmar, C.; Kahn, O. *J. Chem. Phys.* **1993**, *98*, 453.
(60) Cohen, H. D.; Roothaan, C. C. J. *J. Chem. Phys.* **1965**, *43*, 534.
(61) Kamada, K.; Ueda, M.; Nagao, H.; Tawa, K.; Sugino, T.; Shimizu, Y.; Ohta, K. *J. Phys. Chem. A* **2000**, *104*, 4723.
(62) (a) Nakano, M.; Kishi, R.; Takebe, A.; Nate, M.; Takahashi, H.; Kubo, T.; Kamada, K.; Ohta, K.; Champagne, B.; Botek, E. *Comput. Lett.* **2007**, *3*, 333. (b) Nakano, M.; Yamada, S.; Yamaguchi, K. *Bull. Chem. Soc. Jpn.* **1998**, *71*, 845. (c) Nakano, M.; Yamada, S.; Yamaguchi, K. *J. Phys. Chem. A* **1999**, *103*, 3103.
(63) (a) Steiner, E.; Fowler, P. W. *J. Phys. Chem. A* **2001**, *105*, 9553. (b) Steiner, E.; Fowler, P. W. *Chem. Commun.* **2001**, 2220. (c) Fowler, P. W.; Steiner, E.; Jenneskens, L. W. *Chem. Phys. Lett.* **2003**, *371*, 719.
(64) (a) Haddon, R. C.; Fuguhata, T. *Tetrahedron Lett.* **1980**, *21*, 1191. (b) Haddon, R. C. *J. Am. Chem. Soc.* **1979**, *101*, 1722.
(65) Roy, R. K.; Choho, K.; De Proft, F.; Geerlings, P. *J. Phys. Org. Chem.* **1999**, *12*, 503.
(66) (a) Nalwa, H. S.; Mukai, J.; Kakuta, A. *J. Phys. Chem.* **1995**, *99*, 10766. (b) Champagne, B.; Perpete, E. A.; Gisbergen, S. J. A. V.; Baerends, E. J.; Snijders, J. G.; Ghaoui, C. S.; Robins, K. A.; Kirtman, B. *J. Chem. Phys.* **1998**, *109*, 10489. (c) Prabhakar, C.; Bhanuprakash, K.; Rao, V. J.; Balamuralikrishna, M.; Rao, D. N. *J. Phys. Chem. C* **2010**, *114*, 6077. (d) Beratan, D. N. *J. Phys. Chem.* **1989**, *93*, 3915.

(67) (a) Yamaguchi, K. *Self-Consistent Field: Theory and Application*; Elsevier: Amsterdam, The Netherlands, 1990. (b) Yamanaka, S.; Okumura, M.; Nakano, M.; Yamaguchi, K. *J. Mol. Struct.* **1994**, *310*, 205.
(68) Nakano, M.; Kishi, R.; Ohta, S.; Takebe, A.; Takahashi, H.; Furukawa, S.; Kubo, T.; Morita, Y.; Nakasuji, K.; Yamaguchi, K.; Kamada, K.; Ohta, K.; Champagne, B.; Botek, E. *J. Chem. Phys.* **2006**, *125*, 074113.
(69) (a) Becke, A. D. *J. Chem. Phys.* **1993**, *98*, 5648. (b) Lee, C.; Yang, W.; Parr, R. G. *Phys. Rev. B* **1988**, *37*, 785.
(70) (a) Hay, P. J.; Wadt, W. R. *J. Chem. Phys.* **1985**, *82*, 270. (b) Hay, P. J.; Wadt, W. R. *J. Chem. Phys.* **1985**, *82*, 284. (c) Hay, P. J.; Wadt, W. R. *J. Chem. Phys.* **1985**, *82*, 299.
(71) Frisch, M. J.; et al. *Gaussian 03*, revision D.01; Gaussian Inc.: Wallingford, CT, 2004.
(72) Datta, A.; Mallajosyula, S. S.; Pati, S. K. *Acc. Chem. Res.* **2007**, *40*, 213.
(73) (a) Chiodo, S.; Russo, N.; Sicilia, E. *J. Chem. Phys.* **2006**, *125*, 104107. (b) Tian, W. Q.; Ge, M.; Sahu, B. R.; Wang, D.; Yamada, T.; Mashiko, S. *J. Phys. Chem. A* **2004**, *108*, 3806. (c) Drougas, E.; Kosmas, A. M. *Can. J. Chem.* **2005**, *83*, 9. (d) Firdoussi, A.; El.; Esseffar, M.; Bouab, W.; Abbad, J. L.; Mo, O.; Yanez, M. *J. Phys. Chem. A* **2004**, *108*, 10568. (e) Navarro, J. A. R.; Romero, M. A.; Salas, J. M.; Quiros, M.; Bahrauni, J.; El Molina, J. *Inorg. Chem.* **1996**, *35*, 7829.
(74) Dobbs, K. D.; Hehre, W. J. *J. Comput. Chem.* **1987**, *8*, 880.
(75) Cao, X. Y.; Dolg, M. *THEOCHEM* **2002**, *139*, 581.
(76) (a) Cheeseman, J. R.; Trucks, G. W.; Keith, T. A.; Frisch, M. J. *J. Chem. Phys.* **1996**, *104*, 5497. (b) Helgaker, T.; Jaszunski, M.; Ruud, K. *Chem. Rev.* **1999**, *99*, 293. (c) Dios, A. C.; De Laws, D. D.; Odfield, E. *J. Am. Chem. Soc.* **1994**, *116*, 7784.(d) Chesnut, D. B. In *Annual Report on NMR Spectroscopy*; Webb, G. A., Ed.; Academic Press: New York, 1989; Vol. 21.
(77) Giri, S.; Roy, D. R.; Duley, S.; Chakravarty, A.; Parthasarathi, R.; Elango, M.; Vijayaraj, R.; Subramaniam, V.; Islas, R.; Merino, G.; Chattaraj, P. K. *J. Comput. Chem.* **2009**, *31*, 1815.
(78) (a) Jha, P. C.; Rinkevicius, Z.; Agren, H. *ChemPhysChem* **2009**, *10*, 817. (b) Qiu, Y. Q.; Fan, H. L.; Sun, S. L.; Liu, C. G.; Su, Z. M. *J. Phys. Chem. A* **2008**, *112*, 83.
(79) (a) Karna, S. P. *J. Chem. Phys.* **1996**, *104*, 6590. (b) Karna, S. P. *J. Phys. Chem. A* **2000**, *104*, 4735.
(80) Paul, S.; Misra, A. *J. Phys. Chem. A* **2010**, *114*, 6641.
(81) (a) Parr, R. G.; Chattaraj, P. K. *J. Am. Chem. Soc.* **1991**, *113*, 1854. (b) Chattaraj, P. K.; Sarkar, U.; Roy, D. R. *J. Chem. Educ.* **2007**, *84*, 354. (c) Aihara, J. *J. Phys. Chem. A* **1999**, *103*, 7487.
(82) (a) Chemla, D. S.; Zyss, J. *Nonlinear Optical Properties of Organic Molecules and Crystals*; Academic Press: Orlando, FL, 1987; Vols. 1 and 2. (b) Ray, P. C. *Chem. Rev.* **2010**, *110*, 5332.